27.4 A 0.8mm^3 ±0.68psi Single-Chip Wireless Pressure Sensor for TPMS Applications

Manohar B Nagaraju[1], Andrew R Lingley[1], Suresh Sridharan[2], Jingren Gu[1], Richard Ruby[2], Brian P Otis[1]

[1]University of Washington, Seattle, WA,
[2]Avago Technologies, San Jose, CA

This work presents a single-chip sub-mm^3 wireless pressure sensor suitable for tire pressure monitoring. The dynamic behavior and safety of an automobile tire is closely dependent on its inflation pressure: maintaining the manufacturer-recommended pressure is essential to prevent tire failure, provide stability, improve fuel efficiency and tire-life, and to reduce CO_2 emissions [1]. Thus, Tire-Pressure Monitoring Systems (TPMS) have become an essential component in modern vehicles, as stipulated by the National Highway Traffic Safety Administration (NHTSA) in 2006. State-of-the-art TPMS systems currently require a pressure sensor, multiple ICs, several external components, and a crystal on a PCB allowing wireless transmission of tire pressure [2] [3]. In this work, we describe a sub-mm^3 fully integrated wireless pressure sensor including a pressure transducer, interface circuitry, integrated timing reference, and a wireless transmitter integrated into a single die.

Although thin-film bulk acoustic wave resonators (FBAR) have been proposed as mass sensors in prior work [4], here we demonstrate their utility as pressure sensors through minor process modifications. The resonant frequency of an FBAR is sensitive to in-plane stress in the membrane. To first order, this can be expressed by the following equations:

$$f_{resonant} = {}^{V_a}/_{2d}\,, V_a = \sqrt{{}^{C}/_{\rho}}$$

where V_a is the phase velocity of the acoustic wave propagating in the piezoelectric membrane, d is the thickness of the membrane, C is the stiffness matrix and ρ the mass density of the membrane. C and ρ are sensitive to any mechanical stress on (and thus pressure differential across) the piezoelectric membrane. By providing a sealed cavity on one side of an FBAR, application of pressure on the other side introduces a bending stress on the membrane. This changes the resonant frequency of the FBAR, thus creating a relative pressure-to-frequency transducer.

Figure 27.4.1 describes the process flow for fabricating an FBAR-pressure sensor. A common scheme for fabricating FBAR filter membranes is to deposit a sacrificial oxide under an active FBAR membrane that is later removed using wet chemical etching through small release holes [5]. However, this process cannot be used to create a sealed cavity because the release holes directly connect two sides of the membrane making the differential pressure zero. Instead, we create a true sealed cavity by forming a hole using an anisotropic silicon etch and then removing the sacrificial oxide via a second wet etch. The closed cavity for pressure sensing is inherently provided by the hermetically-sealed lid which, in our case, houses the active interface and radio circuitry. The FBAR wafer is fabricated with and without release holes for the reference resonator (left FBAR) and the sensor resonator (right FBAR). The FBAR wafer is then bonded to a Si micro-cap lid wafer that consists of the CMOS circuitry to obtain a hermetically-sealed FBAR-CMOS die. Deep-Reactive-Ion-Etching (DRIE) is used to release the right FBAR membrane and provide a channel for the pressure to access the membrane. The channel diameter is 80μm. After DRIE, the entire wafer is placed in 10:1 deionized water to 49% hydrofluoric acid to remove the sacrificial oxide and release the sensor FBAR (2nd etch). The process flow uses a standard micromachining process throughout, making it commercially viable in mass production.

Both FBAR resonator frequencies are also sensitive to temperature, board/package stress, aging, etc. To cancel these effects to first order, we use two FBARs (reference and sensor FBAR) in the same die. They are in close proximity (10s of microns), allowing precise matching of frequency drift. The reference FBAR also provides a frequency reference for wireless communication.

Figure 27.4.2 shows the block diagram and detail of the sensor interface circuitry. Both core oscillators use the Pierce topology. The resolution of the pressure sensor is set by the minimum oscillator Allan deviation. In an FBAR oscillator, this noise floor is typically dominated by close-in flicker noise. AM-PM (amplitude modulation to phase modulation) conversion arising from non-linear device parasitic dominates the close-in phase noise generation in an FBAR oscillator. A non-linear compensation capacitor was added to reduce this close-in noise as described in [6]. The sensor and reference frequencies are then transmitted using a pseudo-FSK modulation scheme. We use a 630MHz FBAR stack, and a divide-by-two provides the frequency output (315MHz) compatible with short-range devices. The symbol rate for the FSK transmission is a divided down version of the reference frequency, while the frequency deviation provides a measure of the sensor frequency/pressure input. The division ratio dictates the time over which the sensor frequency can be processed/integrated at the receiver. This integration time is fully programmable to trade noise for power consumption (active duty cycle). Typically, integration time for minimum Allan deviation is in the range of 10-100ms for FBAR oscillators. The start-up time of a FBAR oscillator (<10μs) is negligible compared to the time required for minimum Allan deviation.

The interface circuitry was fabricated using the Avago 0.6μm CMOS process. The IC wafer was subsequently bonded with the FBAR wafer to obtain a fully integrated wireless pressure sensor. The total size of the die, including the sensor, reference FBAR and the interface circuitry, is (2.2×0.9×0.4) mm^3. Fig. 27.4.3 shows the SEM of the die and the etch hole. The sensor performance was then characterized by placing it in a controlled pressure chamber. The sensor demonstrates a linear response over a pressure range of 20-70psi, the range of interest for commercial TPMS applications. The sensitivity is approximately 2.2ppm/psi. The frequency changes are mapped to pressure values using a linear fit (Fig. 27.4.4). The maximum error in pressure measurement is ±0.68psi. The time-domain response of the sensor was also characterized (Fig. 27.4.4). The wide bandwidth of the pressure sensor allowed tracking of a sudden pressure drop of 30psi simulating a tire blowout.

The effectiveness of the temperature drift cancellation scheme is shown in Fig. 27.4.5. The responses of the two FBAR track each other and a differential measurement of the frequency results in an error of 3.1ppm over a range of -20 to 70°C. This translates to a maximum error over temperature of 1.4psi in the sensor output over the total 90°C range.

The system consumes 4.7mA from a 2.7V supply with both oscillators and transmitter enabled. The turn-on time of an FBAR oscillator is 4μs and is much less than the integration time required for minimum noise. The duration of one complete frequency transmission for noise optimization is 12ms. Considering a reporting interval of 10s between successive tire pressure readings the average power consumption is 30μW. With a battery capacity of 500mAh available from most-common TPMS batteries, this translates to a lifetime of >5.5 years. Fig. 27.4.6 compares state-of-the-art pressure sensors published and available on the market. Compared to existing solutions, we demonstrate a fullyintegrated wireless miniaturized pressure sensor chip (for TPMS), with the sensor, processing IC, frequency reference, and transmitter in a single batch-fabricated hermetic die.

References:
[1] J. Marek, "MEMS for Automotive and Consumer Electronics," *ISSCC Dig. Tech. Papers*, pp.9-10, 2010.
[2] M. Flatscher, *et al.*, "A Bulk Acoustic Wave (BAW) Based Transceiver for an In-Tire-Pressure Monitoring Sensor Node," *IEEE J. Solid-State Circuits*, vol. 45, no. 1, pp. 167-177, 2010.
[3] Infineon SP37 450kPa Tire Pressure Sensor Datasheet.
[4] M. Nagaraju, *et al.*, "A Fully Integrated Wafer-Scale Sub-mm^3 FBAR-Based Wireless Mass Sensor," *IEEE Frequency Control Symp.*, 2014.
[5] M. Small, *et al.*, "Wafer-Scale Packaging for FBAR-Based Oscillators," *Frequency Control and the European Frequency and Time Forum*, 2011.
[6] K. Sankaragomathi, *et al.*, "A 220dB FOM, 1.9GHz Oscillator Using a Phase Noise Reduction Technique for High-Q Oscillators," *IEEE Radio Frequency Integrated Circuits Symp*., 2013.
[7] J. Wang, *et al*., "Monolithic Integration of Pressure Plus Acceleration Composite TPMS Sensors With a Single-Sided Micromachining Technology," *J. or Microelectromechanical Systems*, vol. 21, no. 2, pp. 284-293, 2012.

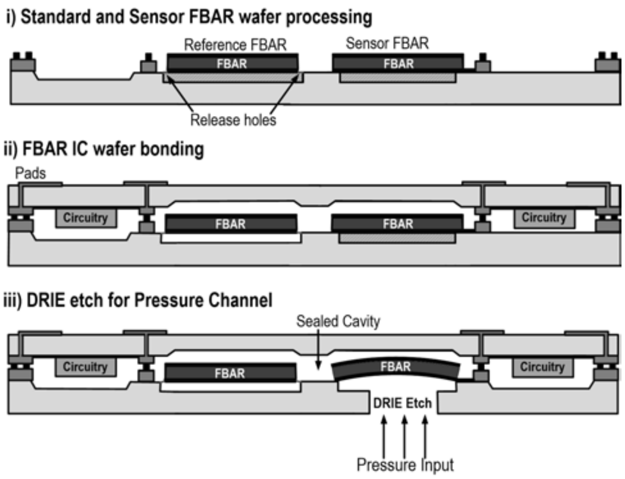

Figure 27.4.1: Process flow for reference and pressure sensor FBAR and final cross section of the FBAR/IC pressure sensor.

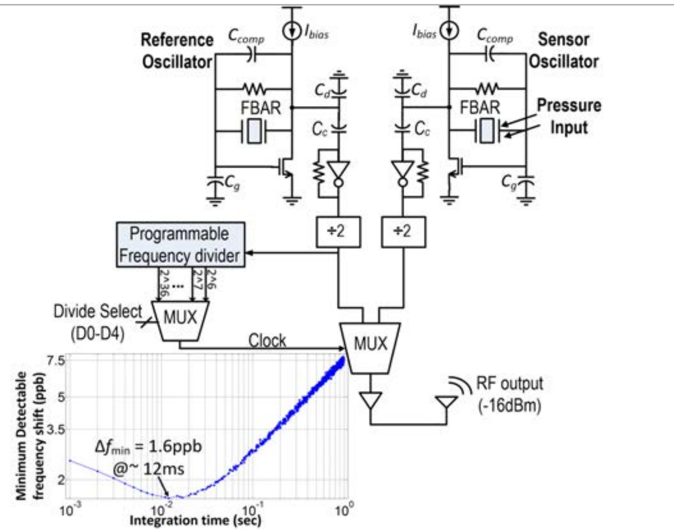

Figure 27.4.2: System block diagram and oscillator circuitry with Allan deviation measurements.

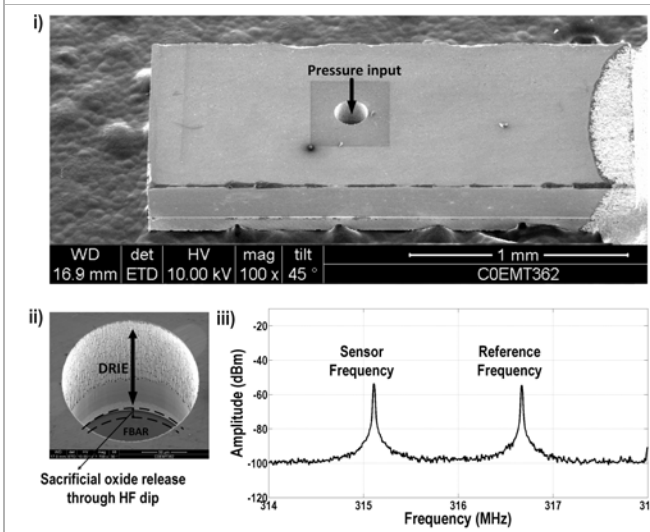

Figure 27.4.3: i, ii) SEM of the FBAR-CMOS die with the etch hole. iii) Sensor output (max hold on a spectrum analyzer) at a distance of 2m.

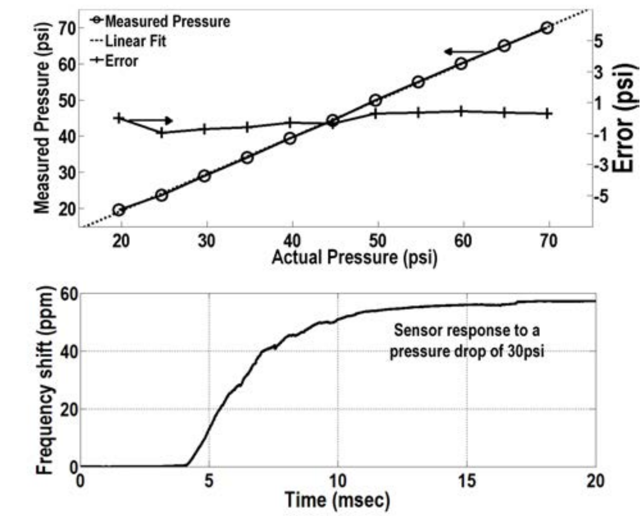

Figure 27.4.4: Sensor calibration curve from 20-70psi and time domain response of sensor simulating a tire blowout (pressure drop of 30 psi).

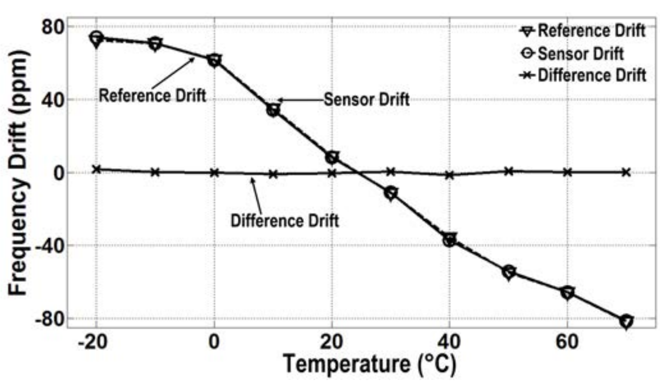

Figure 27.4.5: Frequency drift cancellation due to temperature drift in a differential measurement. Frequency uncertainty is <±1.5 ppm over a range of -20 to 70°C.

	This work	[2] JSSC 2010	[3] Infineon SP37 TPMS Sensor	[7] JMEMS 2012
Size (mm^3)	0.8	998	257	1.92
Integration Comments	Integrates sensor, processing IC and timing reference in a single hermetic die	Sensor, processing IC, transceiver and BAW resonator are integrated through a combination of flip-chip & wire-bonding	Sensor, IC and crystal are integrated in a package	Piezoresistive pressure sensor with no interface circuitry
Power Consumption for a 10s refresh rate	30μW	~9μW	N/A	No interface circuitry
Sensitivity (ppm/psi)	2.2	No sensor measurement reported	N/A	4.7
Resolution (mpsi)	0.72		9	20
Measurement Error (psi)	+/- 0.7 (-20 to 70°C)		+/-1.01 (0-50°C)	N/A
Pressure Range (psi)	20-70		14.5 to 65.26	0-108

Figure 27.4.6: Performance summary and comparison.

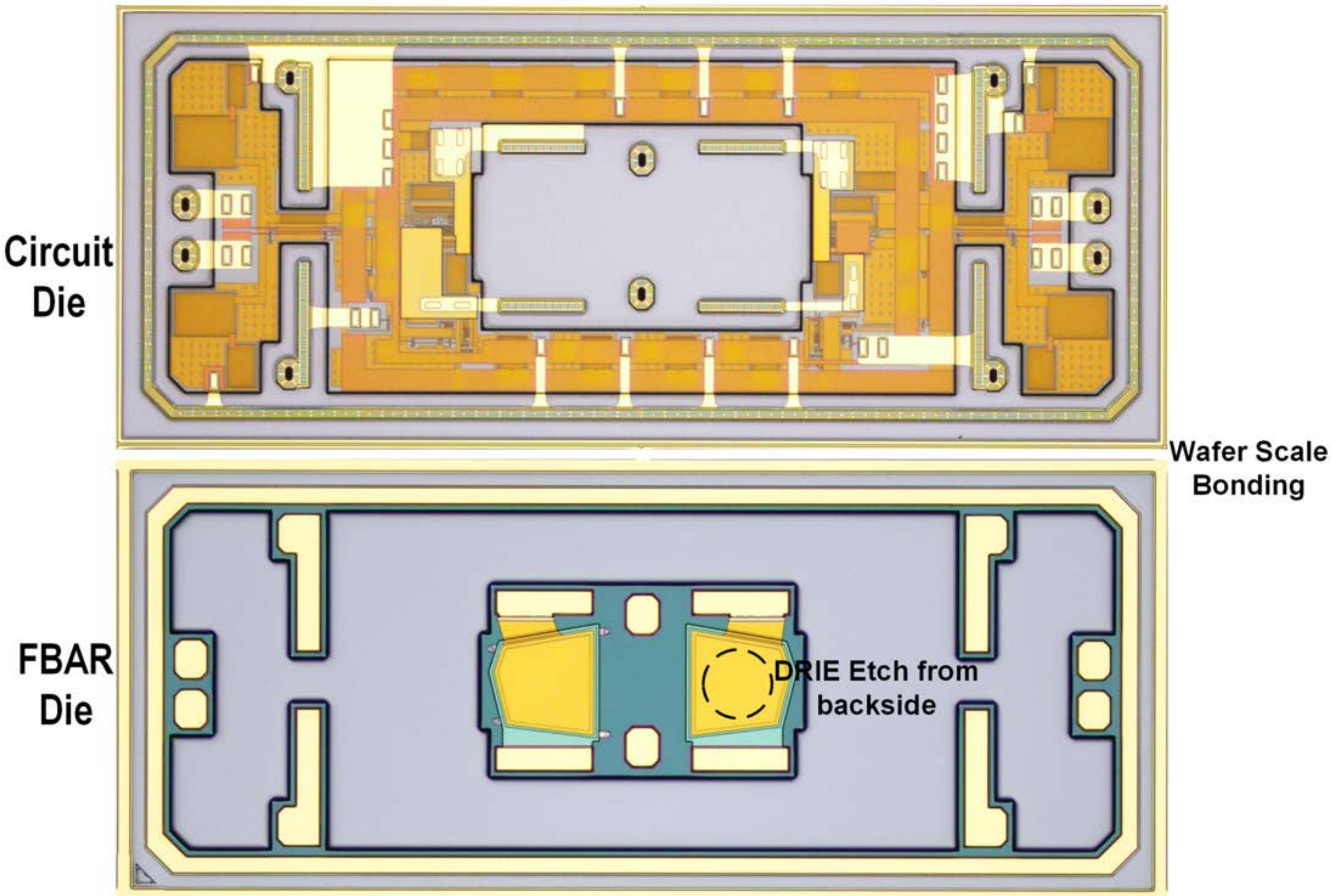

Figure 27.4.7: Die photo of the IC and FBAR wafers before hermetic bonding and etching.